Modeling Land Surface Temperature (LST) and Surface Urban Heat Islands (SUHI) in Taguig City (Philippines) using Material Distribution Derived from Linear Spectral Unmixing of PRISMA Hyperspectral Data

Kim Elijah M. Aguilan[2], Dave Liam T. Ngo[2], Ariel C. Blanco[1,2], Erica Erin E. Elazegui[1,2]

[1]Department of Geodetic Engineering, University of the Philippines, Diliman, Quezon City, Philippines - acblanco@up.edu.ph, eeelazegui@up.edu.ph
[2]Training Center for Applied Geodesy and Photogrammetry, University of the Philippines, Diliman, Quezon City, Philippines - kmaguilan@up.edu.ph, dtngo1@up.edu.ph

Keywords: Land Surface Temperature, Urban Heat Islands, Surface Material Percentage, Hyperspectral

Abstract

As one of the world's fastest developing countries, urbanization in the Philippines occurs at a rapid pace – however, this process has been well established to exhibit negative climatic impacts. This study uses linear spectral unmixing (LSU) of a PRISMA hyperspectral image alongside land surface temperature (LST) data to establish the relationship between material abundance and LST, quantify said relationship through correlation analysis, and identify how materials contribute to surface temperature. Material fraction maps derived from PRISMA were validated using high-resolution PlanetScope imagery, yielding strong agreement for vegetation and built-up areas (R^2 = 0.8420 and 0.9007, respectively). Correlation analysis revealed that vegetation (r = -0.7808 and -0.7794) had strong negative correlations while impervious surfaces, particularly galvanized iron (GI) sheets (r = 0.7260 and 0.7229), exhibited positive correlations with LST and UTFVI calculated using Landsat thermal image. Multilinear regression further quantified these relationships showing that the presence of vegetation and GI sheets produced a strong cooling and warming effect, respectively, on LST; it also identified GI sheets as the most thermally impactful material. These findings demonstrate the effectiveness of combining hyperspectral and thermal remote sensing for UHI analysis and emphasize the need to consider material-specific thermal behavior in planning and building tropical urban environments.

1. Introduction

1.1 Background of the Study

Urbanization is defined as the large-scale movement of populations from rural to more urban settings. In 2018, the United Nations estimated that 55% of the world's population live in urban areas; moreover, urban population is projected to increase to roughly 68% by 2050 (United Nations, 2018). As the growth of metropolitan areas furthers the development of spaces, rapid urbanization has become evident even in third-world countries. With major cities developing facilities, establishments, and infrastructures to service urban lifestyles, the material composition of these urbanized areas begins to change drastically on a localized scale. As this continues to occur, Alcantara et al. (2019) notes that the changes in material composition in the metro have been shown to bear significant effects on the climate of an area.

One key characteristic in describing climate is land surface temperature (LST) which, as the name suggests, is the radiative temperature on the surface of the earth at a specific location. This provides insight for energy and water balance studies by quantifying the "redistribution of energy into latent and sensible heat fluxes" (Hulley et al., 2019). Studies identified contributing factors to changes in LST include the presence or absence of specific types of plants, density of said vegetation, and the amount of solar energy absorbed by surface features such as paved infrastructures and barren soil.
The area's ability to retain or dispel solar energy also diminishes as urban features begin to overtake natural ones. Due to this, LST, especially in densely urbanized areas, has been proven to house higher surface temperatures than that of its surrounding vegetatively dense areas, thus creating Surface Urban Heat Islands (UHIs).

The presence of SUHIs, or UHIs in general, also bears negative consequences on the habitability of cities and causes issues towards the environment and its citizens. Higher surface temperatures impact both local atmosphere and human well-being, causing increased air temperature, higher levels of energy usage in cooling solutions, extreme heat events, and greater risks of illnesses related to heat and pollution (Grimmond, 2007; Ichinose et al., 2008; Mohajerani, 2017; Synnefa et al., 2011; Yang et al., 2015).

1.2 Research Objectives

As surface materials have been proven to directly affect the local climate, this study aims to model UHIs in highly urbanized cities by relating LST with surface material percentage using regression analysis.

To achieve this goal, the specific objectives are to:

1. Estimate and map the percentages of common surface materials by using spectral unmixing of a hyperspectral image;
2. Determine the existing LST-SUHI effect in the area;
3. Provide detailed information regarding the relationship between material abundances and the LST-SUHI as well as what materials can contribute or mitigate this phenomenon.

By identifying specific building materials' contributions to the UHI phenomenon, proper allocation of materials when designing projects can be taken into account, allowing the mitigation of the thermal effects of urbanization. Furthermore,

derivative products such as LST maps of the project area puts UHIs into a local context.

1.3 Scope and Limitations

This study is confined to the City of Taguig, a highly urbanized city in the Metropolitan Manila region. It covers a total area of 47.88 square kilometers, houses 28 barangays with a mixed usage for residential, commercial, and industrial purposes, making it fit for mapping and land use and land cover (LULC) research. Figure 1 shows the varied land use and land cover (LULC) features within the City of Taguig.

Figure 1. The City of Taguig with the satellite image showing the spatial distribution of various land use and land cover features.

Furthermore, the study also focuses on the direct effect of surface material percentage on LST and SUHIs. As such, linear spectral unmixing, correlation, and regression analysis were used as main methodologies. Satellite images, namely, Landsat-9, PRISMA, and PlanetScope acquired in 2023, were utilized for data extraction.

In terms of the feasible methodologies, the study remains restricted to pure pixel sampling from the satellite image due to the inability to conduct in-situ measurements, to the lack of a suitable sample for materials made of concrete, and to mitigate the different effects of specific atmospheric conditions.

2. Review of Related Literature

2.1 LST Estimation and SUHI Detection in Remote Sensing

LST serves as a quantitative basis for analyzing the climate of a specific area and dictates whether the conditions of the climate have deviated from the expected patterns. Chapman et al. (2017) reported that urban growth was found to exhibit large impacts on local temperatures, reaching up to a 5°C increase. They accredited this increase to a combination of climate change and the UHI phenomenon where two notable claims are made. Firstly, climate change, depending on the location, can both increase (e.g. Chicago and Beijing) or decrease (e.g. Paris and Brussels) the effects of heat islands. Secondly, the study notes that after considering both factors of climate change and UHIs, the temperature increase associated with the UHI always turned out to be higher. With these in play, it is only sensible that the study adopts this line of thinking and dissects the factors that influence the LST and SUHIs of an area.

Numerous studies have investigated LST and SUHI dynamics using satellite imageries, with Landsat being one of the most commonly used due to its overall accessibility, long temporal coverage, and appropriate spatial resolution for analysis. Thermal infrared bands from Landsat missions, particularly Landsat 5, 7, 8, and more recently 9, have been utilized to estimate LST using methods such as split-window technique and single-channel algorithm. More importantly, with Landsat Collection 2, Level-2 LST products have been made available, removing the need for atmospheric correction models. These recent innovations have enabled assessments of urban thermal patterns, evaluation of land cover change impacts, and identification of SUHI-vulnerable zones (Ahmed, 2017; Cruz et al., 2020; Estoque et al., 2016; Parastatidis et al, 2017; Sahoo et al., 2022).

2.2 LST-UHI as a Consequence of Land Use and Land Cover (LULC) Change

A study by Alcantara et al. (2019) expresses interest in the same field by exploring the modeling of UHIs itself using ordinary least squares and geographically weighted regression making use of Landsat-8 images. Three of the parameters used are normalized difference vegetation index (NDVI), normalized difference built-up index (NDBI), and surface albedo. NDVI and NDBI are indicators of vegetation and level of urbanization, respectively. Multiple studies have established that the former has a negative relation to LSTs while the latter has positive relation.

Additionally, Alcantara et al. (2019) utilize surface albedos to factor in the incoming solar radiation that is reflected by said surface. Areas in which much of the solar radiation is absorbed instead of reflected indicate the absorption of solar radiation which leads to the trapping of heat. This, in tandem with LST findings, allows for the identification of UHIs as well as their scope of effects.

It is concluded in most studies that UHI intensity is greatly affected by the densification of built environments in urban areas. Some specific examples are in Kandy City and Nuwara Eliya, both tropical mountain regions in Sri Lanka. From 1996 to 2017, positive correlation between the density of built-up lands and mean LST was seen, while the latter has an inverse correlation with the density of agricultural lands; although, the direct effect of which was offset by the initiatives of forest lands preservation led by the government (Raganalage et al., 2018; Raganalage et al., 2019). Both studies show an increase in surface UHI along the urban-rural gradient, solidifying the role of built-up spaces in UHI formation. The same observations are seen in a local mountainous city, as well. Estoque and Murayama (2017) shows that the temperature difference between urban and rural zones rose from 4.0℃ to roughly 8.2℃ in the hilly Baguio City in the Philippines.

Another observation made in the 2017 Baguio City study of Estoque and Murayama (2017) is the temperature difference in areas with artificial impervious surfaces (IS) and green spaces (GS) which increased from 2.7°C to 3.4℃ during the study period of 1987 to 2015. Further studies by Estoque et al. (2016) using Landsat-8 OLI/TIRS data in the three major southeast Asian megacities of Bangkok (Thailand), Jakarta (Indonesia), and Manila (Philippines) also show a strong correlation of LST-IS-GS along the urban-rural gradient. The study implies that a significantly larger GS cover is necessary to combat the LST effects of IS area, especially in areas nearer to city centers as GS density is relatively low within these zones. Importance should also be given to the size, shape, complexity, and aggregation of GS to better combat higher LSTs. Moreover, in Alcantara et al. (2019) and Sahoo et al. (2022), industrial and commercial land use areas are shown to have higher mean LSTs as compared to agricultural areas and water bodies. This is in line with the idea that industrial and commercial areas have more artificial IS as compared to agricultural areas which are rich in GS and vegetation.

2.3 Application of Hyperspectral Data in LST-UHI Assessment

While remotely-sensed data derived from satellite images have been prominent in urban studies, methodologies that can identify and characterize exact features and surface types that consist of these landscapes are still limited. Currently, recent UHI studies in the Philippines usually utilize indices such as NDVI, NDBI, and UTFVI and categorize LULC into four types: built-up, vegetation, barren soil, and surface water.

Alternatively, Priyadarshini et al. (2021) used hyperspectral dataset to determine which specific urban materials aggravate more heat in Kalaburagi, India. This technique uses spectral signatures derived from both satellite images and field measurements for validation. These libraries provide reflectance spectra accurate enough to differentiate urban materials in the study area. It is determined that common materials used in pavement and building construction such as cement, asbestos, and black soil exhibit more heat; thus, effectively exacerbating the UHI phenomenon. In Despini et al. (2021), "modifiable surfaces" such as roofs and parking areas are identified and given higher surface albedos to further understand how common materials can help in mitigating UHIs.

To bridge the gap in existing UHI studies and localize the hyperspectral approach, this study incorporates thermal data from Landsat-9 TIRS/OLI and hyperspectral data from PRISMA. The study identified and provided unique characterization of urban surface material types in relation to thermal hot/cold spots.

3. Methodology

This study builds on existing research on LST and SUHIs by exploring how hyperspectral images can enhance SUHI modeling through detailed detection of material composition percentages.

Figure 2 shows the three main process groups of the study: characterization of LST-UHI, determination of surface material percentage through spectral unmixing, and the analysis of their relationship with each other.

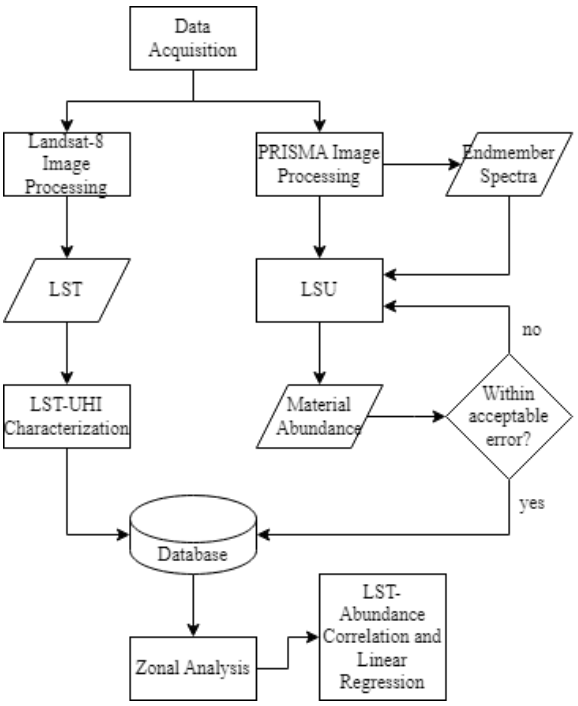

Figure 2. Flowchart of the overall methodology integrating LST-UHI characterization, spectral unmixing, and correlation and regression analysis.

Meanwhile, Table 1 summarizes the remotely sensed datasets used in this study. Landsat-9, PRISMA, and PlanetScope imagery were acquired to derive LST, perform spectral unmixing for material percentages, and validate results, respectively. It should be noted that the Landsat-9 and PRISMA images were acquired one month apart. While this temporal mismatch may introduce minor discrepancies due to seasonal dynamics, the short gap during the dry season minimizes substantial changes in land cover.

Satellite Imagery	Date of Acquisition	Spatial Resolution	Purpose
Landsat-9	March 12, 2023	30 m	LST calculation
PRISMA	April 20, 2023	30 m	Spectral unmixing to generate material percentages
PlanetScope	March 22, 2023	3 m	Data validation

Table 1. Summary of remotely-sensed datasets.

Each satellite product was used to provide different parameters to the dataset. Landsat-9 utilizes Operational Land Imager 2 (OLI-2) and the Thermal Infrared Sensor 2 (TIRS-2) to provide thermal data through its Collection 2 Level 2 Science Products. (USGS, 2022). PRISMA on the other hand collects data across 236 spectral bands allowing for precise identification and characterization of various materials and features on the Earth's surface (ASI, 2020). Finally, PlanetScope provides high resolution satellite images at 3 - 5 meters that may be used for data validation (Planet Labs, 2022)

3.1 Image Pre-Processing

The following initial steps were taken to prepare the data sets for analysis:

The formula applied to the acquired Landsat-9 Level 2 Surface Temperature (ST) Science Product to calculate the final land surface temperature (LST) was:

$$T_S = \left(0.00341802 \ * T_i\right) + 149.0 \quad (1)$$

where T_S = Final LST in Kelvin;
T_i = Initial LST in Kelvin;
0.00341802 is the scale factor;
149.0 is the offset value.

For PRISMA imagery, ground control points were established to georeference and align the PRISMA image to the acquired boundary layer as validated through PlanetScope. Second, minimum noise fraction (MNF) analysis was performed to remove unwanted variability and enhance signal-to-noise ratio in the image.

For the purpose of this study, each component was visually inspected and only the first 16 MNF bands were used and reverted back through the inverse MNF algorithm, producing the denoised image. The resulting forward MNF output also served as the input for the pixel purity index (PPI) algorithm, a process necessary in choosing pure pixels for endmember spectra collection. These processes are summarized in the following flowchart in Figure 3.

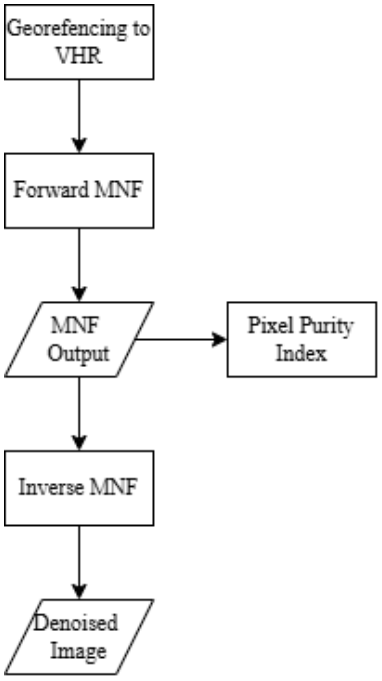

Figure 3. Pre-processing steps for the acquired PRISMA image.

3.2 UTFVI Calculation

UTFVI is an LST-based index used to provide quantitative and qualitative assessment of the severity of the presence of UHIs within a specific study area. This index is computed by using the following formula:

$$UTFVI = \frac{T_S - T_{mean}}{T_S} \quad (2)$$

where T_S = LST of a specific point in Kelvin;
T_{mean} = Mean LST within the subject area in Kelvin.

To assess the derived values qualitatively, threshold values to categorize the intensities were set by Ahmed (2017) as shown in Table 2 below:

Urban Thermal Field Variance Index	Presence of UHI Phenomenon
<0.000	None
0.000-0.005	Weak
0.005-0.010	Moderate
0.010-0.015	Strong
0.015 - 0.020	Stronger
> 0.020	Strongest

Table 2. Qualitative categories of UHI intensity based on UTFVI.

3.3 Linear Spectral Unmixing

To conduct linear spectral unmixing, the following workflow illustrated in Figure 4 was followed:

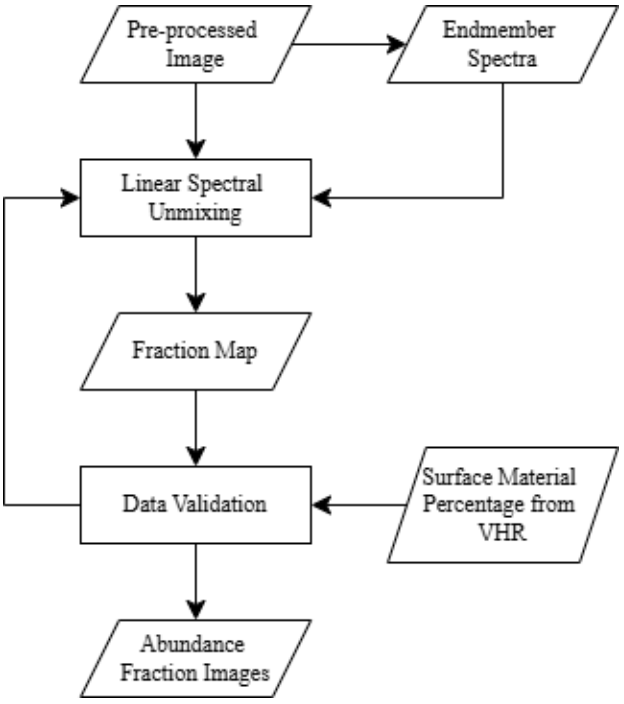

Figure 4. Process flowchart for surface material percentage determination using linear spectral unmixing.

Prior to conducting the actual unmixing, a spectral library was built by employing the Pixel Purity Index (PPI) to identify suitable sample pixels within the image that are made up of a single material. These pure pixel samples were taken per endmember. Using this, a pixel with high PPI value indicates a higher likelihood of being dominated by a single material, whereas a low PPI value suggests heterogenous pixels. Table 3 shows the following endmembers that were utilized for the unmixing:

Surface Class	Specific Endmembers
Vegetation	Aquatic Vegetation Grass Tree
Impervious Materials	Asphalt Galvanized Iron (GI) Sheets
Soil	Barren Soil
Water	River Water

Table 3. Endmembers used in the spectral unmixing algorithm.

Once the spectral library was built, the unmixing decomposed mixed pixel spectra into its constituent endmembers and provided abundance fractions within each pixel, based on the assumption that each mixed pixel's spectral signature is a linear combination of the spectral signatures of the pure endmembers present in it.

To validate its outputs, pixel-based unsupervised classification using the ISODATA algorithm was performed onto the PlanetScope image with classifications of vegetation, asphalt, GI sheets, soil, and water. Using a 150 x 150 meter fishnet grid, the total percentage cover of both vegetation and impervious surfaces were computed. This, together with the relative abundance of each endmember for water, vegetation and impervious materials as derived from PRISMA, were extracted to serve as validation samples. Linear regression analysis was performed to determine the coefficient of determination between the two datasets.

3.4 LST-UTFVI vs Surface Material Abundance

A total of 6 000 random points were generated throughout the study area using a simple random sampling approach. At each point, data were extracted for LST, UTFVI, and the percentage cover of vegetation, asphalt, GI sheets, soil, and water. These datasets were then analyzed using correlation and regression analysis to assess the relationships between surface material abundance and thermal characteristics.

4. Results and Discussion

4.1 Linear Spectral Unmixing

Refining the LSU processes for the study consisted of a series of trial-and-error in order to determine the optimal configuration that best suits the image. Generally speaking however, each trial utilized similar configurations of constrained unmixing with a weight of one. Significant changes and milestones to the process are further discussed below.

The first iteration was the most straightforward approach towards unmixing, utilizing a library of eight endmembers (including an additional concrete endmember) derived from the pure pixels of the image. This provided an image that was able to detect the presence of the majority of materials in a pixel; up to 2 or 3 of the primary materials within said pixel – however the numerical percentage showed the presence of large negative values which should not be the case when assessing the percentage abundance of materials.

The presence of large and negative values in linear spectral unmixing, while not uncommon, is documented by L3Harris Technologies to be a sign of either missing endmembers crucial to the unmixing or samples not well characterized enough to act as bases for the unmixing. A sample area and the results of this iteration of unmixing are shown in Figure 5.

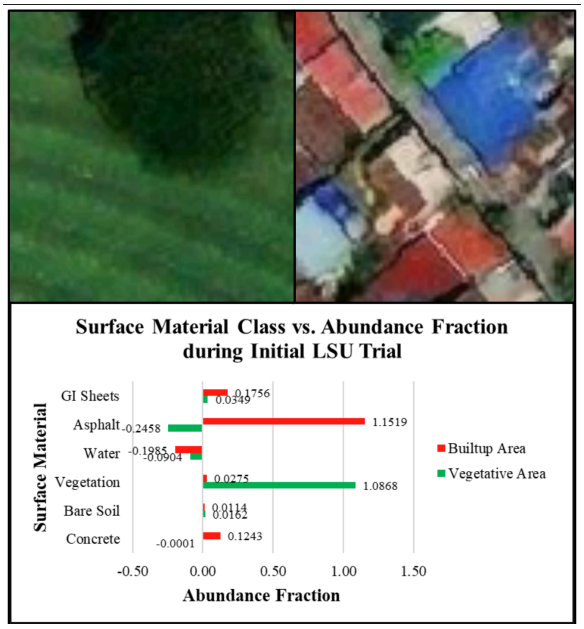

Figure 5. Surface material abundance fractions of the initial implementation.

It was further noted that GI sheets which should have been the majority composition, were not detected in the unmixing. Upon investigation, significant differences in the spectral signatures of differently painted roofs were observed, specifically in the visible and infrared spectrum. Due to these differences, a general sample of GI sheets performed poorly, as the created sample spectra attempts to compensate for these differences, effectively removing a defining feature of the endmember's spectral signature.

In response, a total of four GI sheet endmembers were temporarily added to the spectral library namely neutral (N), red (R), green (G), and blue (B) samples in order to cover the different possible colors of roofs. This had now allowed for better detection of the GI sheet endmembers when recombined to act as a general indicator for GI sheets. In addition to this, asphalt and concrete were also found to be problematic endmembers, exhibiting similar spectral signature patterns (Figure 6), which the unmixing often could not differentiate – thus, these endmembers were consolidated as one.

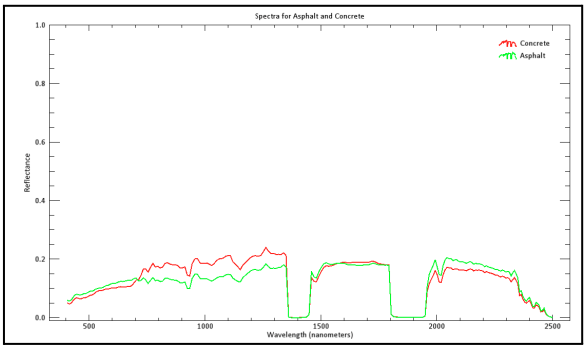

Figure 6. Comparison of the spectral signatures between asphalt and concrete endmembers.

The researchers further noted that separating the unmixing of vegetation and built-up areas using the normalized difference

vegetation index (NDVI) to provide initial categorization of the image, the unmixing resulted in more sensible and acceptable values. A sample area and the results of this iteration of unmixing are shown in Figure 7.

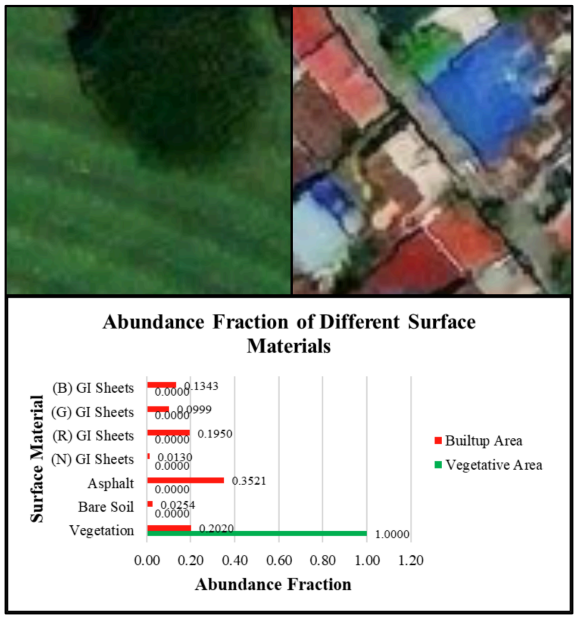

Figure 7. Surface material abundance fractions after initial broad classification and separated GI sheet endmembers.

At this stage of the iterative process, the researchers noted two criteria that led to deeming the output as satisfactory: (1) the unmixing no longer returned the large negative values found in prior iterations, indicating that the quality of the sample endmembers are sufficient; and (2) the results of the unmixing sums up to 1, providing a good indicator of the respective material percentages.

The unmixing of these materials resulted in the fraction images shown in Figure 8. These images of the study area showcase the spatial distribution of each material. Vegetative areas are clustered together while impervious materials dominate the majority of the city. Light-colored pixels correspond to higher amounts of material abundance; conversely, lower abundance corresponds to darker-colored areas, with a range of 0-100%.

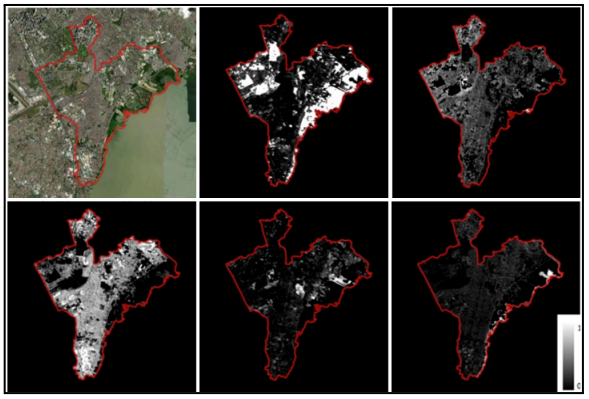

Figure 8. Spatial distribution of surface materials. within the study area. Fraction images from the top-left position in a clockwise direction: (a) True-color image, (b) vegetation, (c) asphalt, (d) water, (e) soil, (f) GI sheets.

4.2 Spatial Distribution of LST-UHI

The LST values of Taguig City ranged widely from 29.17°C to 50.32°C on March 12, 2023. The lowest LST values were found around the vegetative coastal areas along Laguna de Bay while the highest values were located in large industrial and densely populated residential areas. These were then used to compute for UHI and represented graphically in Figure 9.

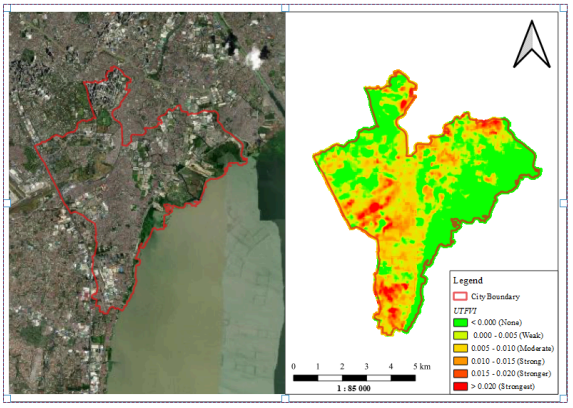

Figure 9. UHI presence in Taguig City on March 12, 2023.

A zonal statistics tool was also used to compute the mean urban thermal field variance index (UTFVI) values of the city's barangays. Figure 10 shows that the lowest UTFVI values are along the vegetative coastal areas, in agreement with the LST findings above. Although the majority of the city is residential in nature, higher mean UTFVI values were found in densely populated residential areas as compared to localities with mixed vegetation and impervious surfaces (e.g., barangays with high-end villages that contain golf courses and pocket parks).

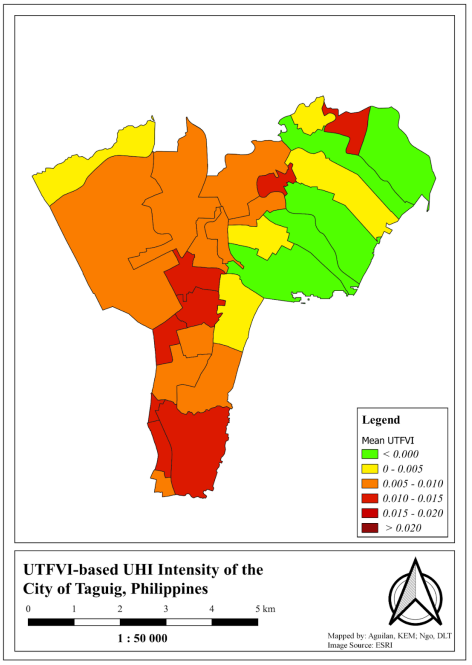

Figure 10. UHI presence in Taguig City per barangay.

4.3 Correlation between LST-UHI and Surface Material Percentage

Using random points within the subject area, the percent cover of the endmembers versus LST and UHI were analyzed independently. Table 4 shows that relative to LST, a strong negative correlation to vegetation was found with values of -0.7808 and an R-squared value of 0.6096 – indicating that 60.96% of variability in LST can be explained by the presence of vegetation. On the other hand, notable positive correlations with both asphalt and GI sheets, with correlation values of 0.4868 and a much stronger 0.7260, respectively. Coefficient of determination values for asphalt and GI sheets are 0.2369 and 0.5271, respectively. Soil and water have significantly weaker correlation coefficients of -0.2588 and -0.3376, respectively, alongside weak coefficients of determination values of 0.0670 and 0.1139, respectively.

Endmember	R	R^2
Vegetation	-0.7808	0.6096
Soil	-0.2588	0.0670
Water	-0.3376	0.1139
Asphalt	0.4868	0.2369
GI Sheets	0.7260	0.5271

Table 4. Coefficients of correlation and determination of endmembers to LST.

In respect to UTFVI, the general trend still remains the same. Vegetation was shown in Table 5 to have a strong negative correlation with UTFVI, with a correlation coefficient of -0.7794 and a coefficient of determination value of 0.6075, Conversely, significant positive correlations were found between asphalt and GI sheet materials with correlation coefficient values of 0.4836 and 0.7229, respectively. With coefficients of determination of 0.2339 and 0.5226, respectively. Finally, soil and water both have negative correlations with UTFVI with values of -0.2555 and -0.3419, respectively, alongside weak coefficient of determination values at only 0.0653 and 0.1169, respectively.

Endmember	R	R^2
Vegetation	-0.7794	0.6075
Soil	-0.2555	0.065
Water	-0.3419	0.1169
Asphalt	0.4836	0.2339
GI Sheets	0.7229	0.5226

Table 5. Coefficients of correlation and determination of endmembers to UTFVI.

4.4 Multiple Linear Regression (MLR) Model for LST and UTFVI

The variables with the strongest and significant correlation namely abundance fractions for vegetation, asphalt, and GI sheets were used in creating the linear regression model for both LST and UTFVI. As indicated by the p-values, all variables used in the regression model were significant. The RMSE values for the two models were 1.4280 and 0.0806, respectively. Agreeing with the results derived above, vegetation fraction has negative correlation with both LST and UTFVI; meanwhile, asphalt and GI sheet fractions have strong positive correlation with the two variables. Table 6 summarizes the results of the MLR modeling of both LST and UTFVI.

Parameter	LST (in Celsius)	UTFVI
Multiple R	0.8049	0.8025
R^2	0.6478	0.6440
RMSE	1.4280	0.0806
Intercept	40.1620	-0.0067
P-value	0.0000	0.0000
Vegetation Coefficient	-2.0999	-0.0068
P-value	0.0000	0.0000
Asphalt Coefficient	4.9656	0.0156
P-value	0.0000	0.0000
GI Sheets Coefficient	6.0401	0.0189
P-value	0.0000	0.0000

Table 6. Results of the multiple linear regression modeling of LST and UTFVI.

5. Conclusions and Recommendations

The insights from the results of this study outline the flaws and possible improvements that can be made in the implementation of urbanization. Firstly, it shows that there is definite evidence of the heat-retentive abilities of galvanized iron sheets, which are prevalent as roofing materials of both commercial buildings and residential houses. Conversely, it reaffirms the claims made by UHI studies regarding the cooling effect that vegetative areas have on land surface temperature, and showcases the cooling ability of green spaces. Together, these findings showcase the primary flaw in the country's current system of urbanization: its built-up features, specifically buildings and houses, are built too densely, with hardly any space between them, and without room for green spaces to mitigate this.

This urbanization pattern is not unique to Metro Manila. Emerging cities like Baguio, Cebu, Iloilo, and Davao, while currently retaining relatively larger peri-urban green spaces, are undergoing rapid urbanization and densification. By replicating this analysis, experts can gain comparative insights across cities, showing how variations in urban forms and neighboring landscape patterns can influence UHI intensity.

The researchers recommend the following: firstly, the use of a larger subject area in order to gain an understanding of the phenomenon at a larger scale. As it stands, Taguig City was used mainly due to the presence of mixed land cover; however, Taguig is still situated in the heart of the metro, locked amongst other major cities. By utilizing a larger subject area, the study allows for analysis of areas that transition into the greener more rural areas outside of Metro Manila as well as the potential for other material samples for more elusive endmembers such as concrete and wood. Alongside this, on-ground samples and verification may also further open other endmembers that have been limited by the PPI-based methodology. Furthermore, other robust analysis methods such as geographically weighted regression (GWR) may also provide further sub-citywide insights from the data. Finally, when available, the researchers believe that higher spatial resolutions of hyperspectral images

will greatly aid in the advancement of the study – allowing for more potential material samples as well as more in-depth results from the unmixing process.

Acknowledgements

We would like to express our deepest appreciation to all those who have supported this study. To the UP Department of Geodetic Engineering, for their resources and relentless efforts to cultivate an intellectually stimulating curriculum. To Mr. Patrick Ostrea, through the Leocadio and Jocelyn Ostrea Thesis Support Grant, for the financial assistance they have granted. To Mr. Ricardo Ngo, Ms. Aileen Ngo, and Mr. Rodolfo Aguilan, for their unconditional love, encouragement and belief in our abilities.

References

Agenzia Spaziale Italiana (ASI). 2020. *PRISMA products specification document*.

AhmedSaada, Saada. 2017. Assessment of urban heat islands and impact of climate change on socioeconomic over Suez Governorate using remote sensing and GIS techniques. The Egyptian Journal of Remote Sensing and Space Science. 21. 10.1016/j.ejrs.2017.08.001.

Alcantara, C., Escoto, J., Blanco, A., Baloloy, A., Santos, J., & Sta. Ana, R. 2019. Geospatial assessment and modeling of urban heat islands in Quezon City, Philippines using OLS and geographically weighted regression. The International Archives of Photogrammetry, Remote Sensing, and Spatial Information Sciences, XLII-4/W16.

Chapman, S., Watson, J., Salazar, A., Thatcher, M., & McAlpine, C. 2017. The impact of urbanization and climate change on urban temperatures: a systematic review. Landscape Ecology, 32(10), 1921-1935.

Cruz, J.A., Santos, J.A., & Blanco, A. 2020. Spatial disaggregation of Landsat-derived land surface temperature over a heterogeneous urban landscape using PlanetScope image derivatives. The International Archives of Photogrammetry, Remote Sensing, and Spatial Information Sciences, XLIII-B5-2020.

Despini, F., Ferrari, C., Santunione, G., Tommasone, S., Muscio, A., & Teggi, S. 2021. Urban surface analysis with remote sensing data for the evaluation of UHI mitigation scenarios. Urban Climate, 35(2021), 100761.

Estoque, R., & Murayama, Y. 2017. Monitoring surface urban heat island formation in a tropical mountain city using Landsat data (1987–2015). ISPRS Journal of Photogrammetry and Remote Sensing, 133, 18-29. doi: 10.1016/j.isprsjprs.2017.09.008

Grimmond, S. 2007. Urbanization and global environmental change: local effects of urban warming. The Geographical Journal, 173(1), 83-88. doi: 10.1111/j.1475-4959.2007.232_3.x

Hulley, G. C., Ghent, D., Gottsche, F., Guillevic, P., Mildrexler, D., & Coll, C. 2019. Land surface temperature. Taking the Temperature of the Earth: Steps towards Integrated Understanding of Variability and Change, 57-127. doi: 10.1016/B978-0-12-814458-9.00003-4

Ichinose, T., Matsumoto, F., & Kataoka, K. 2008. Chapter 15: Counteracting urban heat islands in Japan. Urban Energy Transition, 365-380. Amsterdam, Netherlands: Elsevier.

Mohajerani, A., Bakaric, J., & Jeffrey-Bailey, T. 2017. The urban heat island effect, its causes, and mitigation, with reference to the thermal properties of asphalt concrete. Journal of Environmental Management, 197, 522-538. doi: 10.1016/j.jenvman.2017.03.095

Parastatidis, D., Mitraka, Z., Chrysoulakis, N., & Abrams, M. 2017. Online global land surface temperature estimation from Landsat. Remote sensing, 9(12), 1208.

Planet Labs. 2022. *Planet Imagery Product specifications.*

Priyadarshini, K., Sivashankari, V., Shekhar, S., & Balasubramani, K. 2021. Examining land surface temperature from agglomerative spectra using hyperspectral dataset. Sustainable Climate Action and Water Management. doi: 10.1007/978-981-15-8237-0_17

Ranagalage, M., Dissanayake, D., Murayama, Y., Zhang, X., Estoque, R., Perera, E., & Morimoto, T. 2018. Quantifying surface urban heat island formation in the world heritage tropical mountain city of Sri Lanka. ISPRS International Journal of Geo-Information, 7(9), 341. doi: 10.3390/ijgi7090341

Ranagalage, M., Murayama, Y., Dissanayake, D., & Simwanda, M. 2019. The impacts of landscape changes on the annual mean land surface temperature in the tropical mountain city of Sri Lanka: a case study of Nuwara Eliya (1996-2017). Sustainability, 11(19), 5517. doi: 10.3390/su11195517

Sahoo, S., Majumber, A., Swain, S., Gareema, Pateriya, B., & Al-Ansari, N. 2022. Analysis of decadal land use changes and its impacts on urban heat island (UHI) using remote sensing-based approach: a smart city perspective. Sustainability, 14, 11892. doi: 10.3390/su141911892

Synnefa, A., Karlessi, T., Gaitani, N., Santamouris, M., Assimakopoulos, D.N., & Papakatsikas, C. 2010. Experimental testing of cool colored thin layer asphalt and estimation of its potential to improve the urban microclimate. Building and Environment, 46(1), 38-44. doi: 10.1016/j.buildenv.2010.06.014

United Nations. 2018. World urbanization prospects: the 2018 revision [key facts]. New York City, NY.

U.S. Geological Survey (USGS). 2022. *Landsat 9 data users handbook*.

Yang, J., Wang, Z., & Kaloush, K. 2015. Environmental impacts of reflective materials: is high albedo a 'silver bullet' for mitigating urban heat island. Renewable and Sustainable Energy Reviews, 47, 830-843. doi: 10.1016/j.rser.2015.03.092